Available online at www.sciencedirect.com
ScienceDirect
Journal of Catalysis 253 (2008) 159–166
JOURNAL OF CATALYSIS
www.elsevier.com/locate/jcat

Hydrogenation of α, β unsaturated aldehydes over polycrystalline, (111) and (100) preferentially oriented Pt nanoparticles supported on carbon

J.C. Serrano-Ruiz [a], A. López-Cudero [b], J. Solla-Gullón [b], A. Sepúlveda-Escribano [a,*], A. Aldaz [b], F. Rodríguez-Reinoso [a]

[a] *Departamento de Química Inorgánica, Universidad de Alicante, Apartado 99, 03080 Alicante, Spain*
[b] *Instituto Universitario de Electroquímica, Universidad de Alicante, Apartado 99, 03080 Alicante, Spain*

Received 20 June 2007; revised 21 September 2007; accepted 12 October 2007

Available online 26 November 2007

Abstract

The influence of the shape/surface structure of Pt nanoparticles on the selective hydrogenation of crotonaldehyde and cinnamaldehyde has been studied. (111) and (100) preferentially oriented Pt nanoparticles (10 nm) as well as polyoriented Pt nanoparticles (3 nm) were synthesized, characterized (by TEM, cyclic voltammetry and adsorption microcalorimetry) and their catalytic properties evaluated. TEM analysis provided information about the size and shape of the Pt nanoparticles, whereas cyclic voltammetry allowed gaining qualitative and quantitative information about their surface structure. Thus, small Pt nanoparticles (≈3 nm) were revealed to have a polyoriented surface, containing high ratio of corner and edges atoms to terrace atoms, whereas large Pt nanoparticles (≈10 nm) were shown to have larger Pt domains with (100) and (111) surface structures. Microcalorimetric results for CO adsorption showed higher values of initial heat for polyoriented Pt/C compared to preferentially oriented samples, thus accounting for a higher amount of highly unsaturated surface platinum atoms for Pt/C, in agreement with cyclic voltammetry. The catalytic performances of the samples showed a strong structure-sensitive character for both reactions, with TOF values following the trend Pt(100)/C > Pt(111)/C > Pt/C. Moreover, Pt(111)/C showed higher selectivities to unsaturated alcohol than Pt(100)/C and Pt/C samples.

Keywords: Nanoparticles; Platinum; Unsaturated aldehydes; Preferential surface orientation

1. Introduction

The influence of the surface structure of a metal particle on its catalytic and electrocatalytic properties has been extensively reported [1–3]. Nevertheless, in the case of nanoparticles, the effect of the surface structure has been generally related to the so-called "size effect." Thus, some reactions have been shown to be strongly dependent on the particle size, whereas others are independent of the particle size. Boudart, in 1969, classified the first type of reactions as structure sensitive, and the second type as structure insensitive [4]. Later studies related the structure sensitive character of a given reaction to the structure sensitive character of the chemical bond formed between the reactant and the catalyst surface, the strength of which is affected by the local surface structure (relative concentration of steps, terraces, etc.) [5]. Nevertheless, the effect of metal nanoparticle size on catalytic or electrocatalytic activities is better understood at present than the influence of the shape/surface structure, since size control of the nanoparticles has generally been easier than shape/surface structure control. In spite of that, some papers have demonstrated that it is possible to synthesize quasi-monodispersed Pt nanoparticles of controlled particle shape and that the catalytic or electrocatalytic properties of these nanoparticles are under shape/surface structure control. Thus, El-Sayed et al. have reported about the effect of the shape of Pt nanoparticles on their catalytic properties [6–11]. Reactions such as propylene hydrogenation, electron-transfer and Suzuki reactions have revealed the importance of controlling the shape of the nanoparticles. Somorjai et al. have also shown the importance of the shape/surface structure using ethylene hydrogenation and carbon monoxide adsorption and oxidation as surface reaction probes [12,13]. Aldaz et al. have

* Corresponding author. Fax: +34 965 90 34 54.
E-mail address: asepul@ua.es (A. Sepúlveda-Escribano).

0021-9517/$ – see front matter
doi:10.1016/j.jcat.2007.10.010

also reported the influence of the particle shape/surface structure on the electrocatalytic properties of Pt nanoparticles using ammonia oxidation and carbon monoxide adsorption–oxidation as model reactions [14,15].

From the point of view of the synthesis, and since the pioneer work of El-Sayed et al. [16], some contributions have appeared in relation to the preparation of nanoparticles with controlled shape [17–19]. These new methodologies have been mainly focused on the synthesis of Au and Pt nanoparticles with preferential shape/surface structure, due to the great number of reactions where this kind of materials can be employed.

An interesting model reaction is the hydrogenation of α,β-unsaturated aldehydes (acrolein, crotonaldehyde, cinnamaldehyde, etc.). Here, the selective hydrogenation of the carbonyl group, which is preferred because the unsaturated alcohols are valuable intermediates for the production of perfumes and pharmaceuticals, is very complicate, and with usual hydrogenation catalysts complete hydrogenation (both C=C and C=O groups) to yield the primary alcohol or selective hydrogenation of the olefin bond to give the saturated aldehyde are often obtained. Low selectivity toward crotyl alcohol is generally obtained with Pt supported catalysts, although it can be increased by using different approaches, such as an increment of the platinum particle size and by the use as support of a reducible oxide such as TiO_2 [20–22]. An increase in selectivity toward the unsaturated alcohol in the liquid phase hydrogenation of crotonaldehyde over Pt nanoparticles supported on SiO_2 and Al_2O_3 (from 9 to 35%) has been obtained by increasing their particle sizes (from 2 to 6 nm) [21]. It has been shown that the selectivity to the primary products, butyraldehyde and crotyl alcohol, critically depends on the Pt particle size [20]. The presence of a high fraction of Pt(111) surfaces in large Pt nanoparticles favors the adsorption of crotonaldehyde via the carbonyl bond, this leading to its preferential hydrogenation to yield the unsaturated alcohol, the product of interest. On the other hand, both double bonds can be adsorbed without any restriction on Pt(100) and on edges and corners [20]. Under these conditions, the saturated aldehyde is preferentially produced, as the hydrogenation of the C=C bond is favored by both thermodynamic and kinetics reasons. In this way, the synthesis of well-defined shape Pt nanoparticles represents a key point for the design of more active and selective catalysts for this kind of reactions.

Thus, the aim of this work has been to study the hydrogenation of crotonaldehyde and cinnamaldehyde over polyoriented and (100) and (111) preferentially oriented carbon-supported Pt nanoparticles, in order to assess the structure sensitive character of these reactions on platinum.

2. Experimental

Two different protocols have been used to prepare Pt nanoparticles. Polyoriented Pt nanoparticles were synthesized using sodium borohydride as reducing agent in the presence of citrate and using a methodology similar to that previously reported for the preparation of gold seed nanoparticles [23]. An aqueous solution containing 2.5×10^{-4} M H_2PtCl_6 and 2.5×10^{-4} M tri-sodium citrate was prepared. Then, the desired amount of ice cold 0.1 M $NaBH_4$ solution was added all at once with continuous stirring. After 30 min, an appropriate amount of carbon black (Vulcan XC-72) was added to the solution and stirred for 2 h. Finally, two or three NaOH pellets were added to produce the precipitation of the nanoparticles on the carbon support. After complete precipitation, the supported nanoparticles were washed 3–4 times with ultra-pure water.

On the other hand, preferentially oriented nanoparticles were prepared by using the so-called colloidal method [16,17]. Briefly, a variable amount of sodium polyacrylate (PA) aqueous solution was added to a 100 ml of an aged 1×10^{-4} M solution containing the desired Pt precursor. Thus, K_2PtCl_4 was employed for the synthesis of the "(100)-Pt" nanoparticles whereas H_2PtCl_6 was used for the "(111)-Pt" nanoparticles. After 20 min of Ar bubbling, the Pt ions were reduced by bubbling H_2 for 5 min. The reaction vessel was then sealed and the solution was left overnight. After complete reduction (12–24 h), an appropriate amount of carbon (Vulcan XC-72) was added and stirred for two hours. After that, two or three NaOH pellets were added to produce the precipitation of the supported nanoparticles. After complete precipitation, the nanoparticles were washed 3–4 times with ultra-pure water. All samples were prepared to obtain a platinum loading of 5 wt%. The particle size and morphology of all the supported nanoparticle samples were characterized by transmission electron microscopy (TEM).

For the electrochemical experiments, and due to the low Pt metal loading (5 wt%), unsupported Pt nanoparticles were employed. The procedure used for the electrochemical characterization of the nanoparticles has been previously reported [24–26]. The electrochemical measurements were performed in a 0.5 M H_2SO_4 solution at room temperature. Fresh electrolyte solutions were prepared every time an experiment was carried out from Milli-Q water and Merck sulphuric acid. A three-electrode electrochemical cell was used. The electrode potential was controlled using a PGSTAT30 AUTOLAB system. The counter electrode was a gold wire. Potentials were measured against a reversible hydrogen electrode (RHE) connected to the cell through a Luggin capillary. Potentials are quoted versus this reference electrode. Before each experiment, the gold collector was mechanically polished with alumina and rinsed with ultra-pure water to eliminate the nanoparticles from previous experiments.

Differential heats of CO adsorption were measured at 300 K in a Setaram BT2.15D heat-flux microcalorimeter using the method described in detail elsewhere [27]. The microcalorimeter was connected to a high vacuum (base pressure $<10^{-5}$ Torr) volumetric system employing Baratron capacitance manometers for precision pressure measurement (0.5×10^{-4} Torr). The maximum apparent leak rate of the volumetric system (including the calorimetric cells) was 10^{-5} Torr min^{-1} in a system volume of approximately 80 cm^3 (i.e., 10^{-5} μmol min^{-1}). The procedure for microcalorimetric measurements used in this study is described below: each sample (about 0.25 g) was treated ex situ in ultrapure hydrogen (99.999% with further purification, Air Liquide) for 1 h (2 K min^{-1} ramp, 200 ml min^{-1}) at 473 K

and then the sample was purged for 1 h at the same temperature in ultrahigh purity helium (99.999% with further purification, Air Liquide) in order to remove adsorbed hydrogen. Then, it was sealed in a Pyrex NMR tube capsule and broken in a special calorimetric cell [28] after the sample had attained thermal equilibrium with the calorimeter. After the capsule was broken, the calorimetric data were collected by sequentially introducing small doses (1–10 μmol) of CO (99.997% with further purification, Air Liquide) onto the sample until it became saturated. The resulting heat response for each dose was recorded as a function of time and integrated to determine the energy released (mJ). The amount of gas adsorbed (μmol) was determined volumetrically from the dose, equilibrium pressures, and the system volume and temperature. The time required for the pressure to equilibrate in the microcalorimeter after each dose was approximately 1–15 min, and the heat response was monitored for 20–30 min after each dose to ensure that all heat was detected and to allow the heat response to return to the baseline value. The differential heat (kJ mol^{-1}), defined as the negative of the enthalpy change of adsorption per mole of gas adsorbed, was then calculated for each dose by dividing the heat released by the amount adsorbed.

The catalytic behavior of the samples in the vapor-phase hydrogenation of crotonaldehyde (2-butenal [CROALD]) was tested in a microflow reactor at atmospheric pressure under differential conditions. Before the catalytic experiments, the catalysts (around 50 mg) were reduced in situ at 473 K (2 K min^{-1} ramp) under flowing hydrogen (50 ml min^{-1}) for 1 h, and then cooled under hydrogen to the reaction temperature (333 K). Then, the catalysts were contacted with a reaction mixture (total flow: 50 cm^3 min^{-1}; H_2/CROALD molar ratio of 26) containing purified hydrogen and crotonaldehyde (Fluka, >99.5%) prepared by passing a hydrogen flow through a thermostabilized saturator (at 293 K) containing the unsaturated aldehyde. The selectivity to the desired product was calculated as S_i = (moles of product$_i$/moles of products) × 100. The concentrations of the reactants and the products at the reactor outlet were determined by on-line gas chromatography with a Carbowax 20 M 58/90 semicapillary column.

The liquid phase hydrogenation of cinnamaldehyde was carried out in a 300 ml stirred autoclave (Autoclave Engineers, fitted with a system for liquid sampling) at 383 K and at constant pressure of 5 MPa of hydrogen. Before the catalytic experiments, the catalysts (100 mg) were reduced at 473 K (2 K min^{-1} ramp) under flowing hydrogen (50 ml min^{-1}, 99.999%) for 1 h, and suspended in 60 ml of 2-propanol (Riedel-de Haën, 99.9%) previously bubbled with helium for 20 min in order to remove the solved oxygen. After three pressure/vent cycles with helium and three more with hydrogen, the temperature was raised to 383 K under 2 MPa of hydrogen and remained at this temperature for 2 h. Then a mixture of substrate (0.5 ml of cinnamaldehyde, Aldrich 99%) and isopropanol (40 ml) was loaded into the autoclave through an external cylinder (previously flushed with helium and hydrogen) under 8 MPa hydrogen pressure. Zero time was taken at this moment and stirring was switched on (800 rpm). Reaction progress with time was followed taking periodically liquid samples of the reactor. The liquid was analyzed by gas chromatography using a flame ionization detector and a Carbowax 20 M 58/90 semicapillary column.

3. Results and discussion

3.1. Transmission electron microscopy (TEM)

Fig. 1 shows some typical TEM images of the supported and unsupported Pt nanoparticles prepared in this work. Platinum nanoparticles prepared in the presence of citrate, A1 (supported) and A2 (unsupported), show a quasi-spherical shape and an average particle size of 2.5 ± 0.5 nm. In addition, a homogeneous distribution of the Pt nanoparticles on the carbon support can be clearly observed, whereas some agglomeration was detected for the unsupported nanoparticles.

On the other hand, preferentially oriented Pt nanoparticles (images B and C) show well-defined shapes, which can be better observed in the unsupported samples (B2 and C2), as in this condition the influence of the support not only in the contrast of the image but also in the dispersion of the Pt nanoparticles, can be avoided. Thus, the presence of cubic-shaped nanoparticles in clearly shown in image B2, which corresponds to the (100)-Pt nanoparticles. In this sample, particle sizes are around 9 ± 3 nm. The presence of these Pt nanoparticles with a cubic shape is a first indication of the higher presence of (100) Pt atoms on the surface. Images C correspond to (111)-Pt nanoparticles. In the unsupported samples (C2) some tetrahedral and

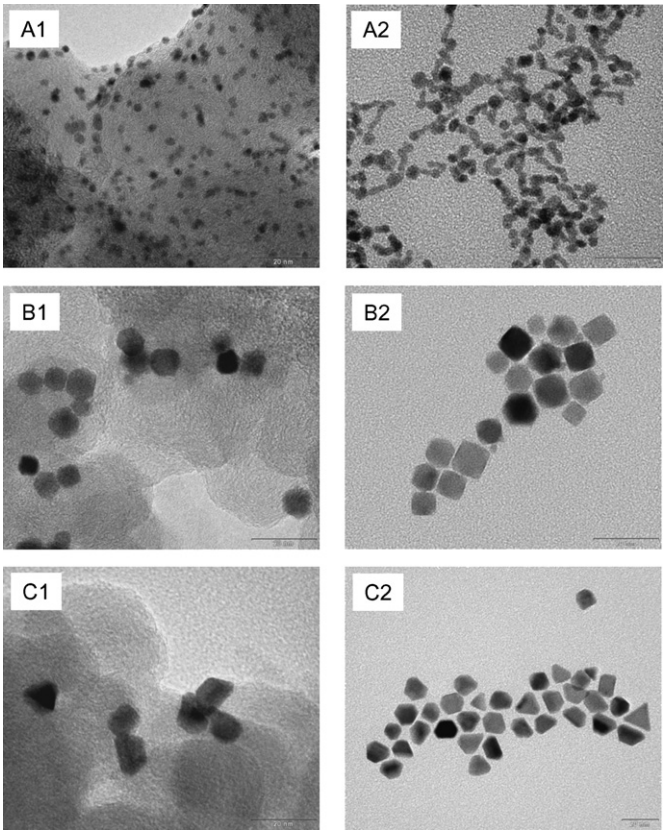

Fig. 1. TEM pictures corresponding to supported (1) and unsupported (2) Pt nanoparticles: polyoriented (A1, A2), preferentially oriented (100) (B1, B2), and preferentially oriented (111) (C1, C2) surface orientation.

hexagonal Pt nanoparticles can be observed, with particle sizes around 10 ± 2 nm. The existence of tetrahedral and hexagonal Pt nanoparticles is again a first evidence of a higher presence of Pt surface atoms with a (111) ordering. It is necessary to remark that all samples were reduced in situ, at 473 K under a hydrogen flow for 1 h before microcalorimetric and catalytic experiments. It was assessed by TEM that no relevant size and shape modification was produced during this pre-treatment.

3.2. Electrochemical characterization

A very good characterization of the structure of a single nanoparticle can be obtained by ex situ HRTEM after simulation of the images [29]. However, the analysis of a statistically significant number of nanoparticles with such a technique seems, currently, unrealistic. Moreover only partial information can be obtained for a given sample of nanoparticles and the real global distribution of surface sites in the nanoparticles could not coincide with the partial distribution found using TEM.

In order to characterize in situ the shape/surface structure of the Pt nanoparticles, a surface sensitive technique or process has to be used. Electrochemistry provides some surface sensitive reactions that can be used as tool to characterize the surface structure. In the case of platinum, it is known that the so-called hydrogen adsorption/desorption process is very sensitive to the Pt surface structure [30] and this fact is put in evidence in the voltammetric profiles shown in Fig. 2. These profiles correspond to the so-called reversible hydrogen adsorption/desorption process on nanoparticles synthesized using different methods. The voltammetric profile works as a fingerprint for any Pt surface. However, in a general way, the direct estimation of the amount of different sites present at the surface is not feasible, since it would require a too complex deconvolution of the voltammograms. Nevertheless with the help of Pt model surfaces it is possible to qualitatively characterize each feature of the voltammetric profile.

Fig. 2 shows the characteristic voltammetric profiles of the different Pt nanoparticles in 0.5 M sulfuric acid. The definition and the symmetry of the adsorption states are indicative of the surface cleanliness. Fig. 2a is characteristic of the small semi-spherical Pt nanoparticles prepared in presence of citrate. The voltammogram looks similar to that reported for polycrystalline platinum electrodes. Thus, the voltammogram shows the presence of adsorption states associated to (110) and (100) sites at 0.12 and 0.27 V, respectively. Moreover, a shoulder around 0.35 V is apparent, being characteristic of (100) terraces. In addition, the unusual adsorption state around 0.5 V, characteristic of small (111) ordered surface domains, can be observed.

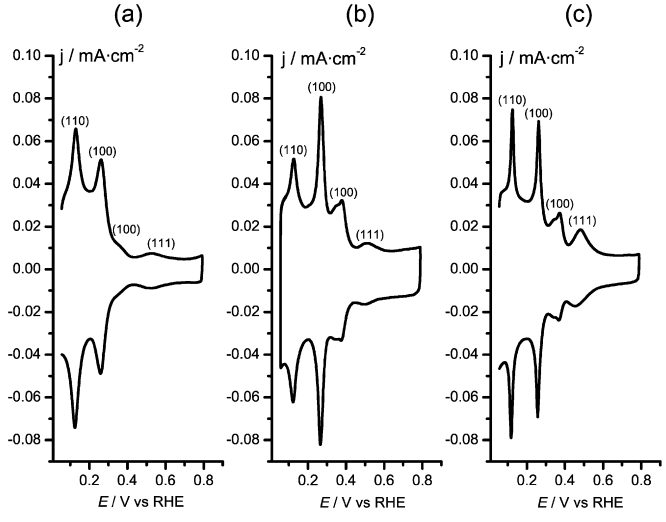

Fig. 2. Voltammograms corresponding to (a) poly, (b) (100), and (c) (111) Pt nanoparticles. Test solution: 0.5 M H_2SO_4, sweep rate 50 mV s^{-1}.

On the other hand, Figs. 2b and 2c show some characteristic voltammetric profiles of "(100)-Pt" and "(111)-Pt" nanoparticles prepared in colloidal solution. For "(100)-Pt" nanoparticles (Fig. 2b) a very sharp peak at 0.27 V is observed. In addition, the well-marked state at 0.37 V, typical of (100) terrace sites, is clearly defined. These results point out that these Pt nanoparticles have a (100) preferential surface structure. Moreover, it is important to note that part of these Pt(100) sites are present at the surface as wide (100) terraces as suggested by the peak at 0.37 V. These electrochemical observations are in agreement with previous results obtained by Ahmadi et al., who pointed out that the nanoparticles obtained are preferentially cubic [16,17].

In the case of the "(111)-Pt" nanoparticles (Fig. 2c), some important features must be noted. First at all, the adsorption state around 0.5 V, characteristic of small (111) ordered surface domains, is much more clearly marked than in the previous cases. This feature is directly related to the presence of bidimensionally ordered (111) domains. On the other hand, the sharp peaks at 0.12 and 0.26 V are also present in the voltammetric profile. These sharp peaks are observed on stepped surfaces vicinal to Pt(111) with monoatomic steps with (110) or (100) sites, respectively. Finally, a well-marked adsorption state at 0.37 V points out that these nanoparticles have also large (100) domains. Similar voltammetric profiles were reported by Attard et al. [31] after a sintering process of the Pt/graphite samples.

The surface structure of similar Pt nanoparticles, both preferentially and poly oriented have been previously electrochemical characterized using the irreversibly adsorptions of Bi and Ge, where Bi is able to identify the presence of Pt(111) surface sites whereas Ge is sensitive to the presence of Pt(100) surface sites [32–35]. In these references, quantitative information about the presence of some characteristic types of surface sites (Pt(111) and Pt(100)) on the surface of Pt nanoparticles was gained. In addition, according to the surface stoichiometry, where each Bi blocks three Pt(111) sites whereas each Ge blocks four Pt(100) sites, information about the percentage of small Pt surface domains as well as the presence of edges and corner surface sites which can not be detected by Bi and Ge and where low coordination Pt atoms are presented, could also be estimated. Thus, in the case of the small polyoriented Pt nanoparticles only a 30–35% of the surface atoms could be detected, whereas for large and preferentially oriented Pt nanoparticles around a 70–90% of the total surface atoms could be identified. These results indicate that, for the small polyoriented Pt nanoparticles, the amount of small surface domains and low coordination surface atoms is significantly higher than

in the case of the preferentially oriented samples. With regard to preferentially oriented samples, irreversible adsorptions of Bi and Ge allowed to detect only the 70% of surface platinum sites in the case of Pt(111), whereas this value was increased until a level of 90% for Pt(100). This finding reveals the presence of a higher amount of small domains and low coordination surface platinum atoms in the case of Pt(111)/C catalyst, which seems to be in agreement with the voltammetric results discussed above.

3.3. CO adsorption microcalorimetry

Fig. 3 plots the evolution of the differential adsorption heats with CO coverage for catalysts previously reduced at 473 K. It can be observed in all cases that the heat of adsorption decreases as the CO coverage increases, this being due to adsorption on weaker sites and/or to interactions between adsorbed species. The drastic drop in the differential heat at higher coverage is indicative of saturation of the accessible platinum metallic surface sites. The polycrystalline Pt/C catalyst showed an initial adsorption heat of 115 kJ mol^{-1}, which is in good agreement with the value reported by Silvestre-Albero et al. [36] for a 0.2 wt% Pt/C catalyst prepared by a conventional impregnation method, and using H_2PtCl_6 as platinum precursor. Adsorption heats hardly decreased until a coverage of 12 μmol g^{-1}, and then they suddenly dropped to the weakly adsorbed CO level, taken as 40 kJ mol^{-1} [37]. Consequently, the saturation coverage for this sample (amount of CO necessary to totally saturate the platinum surface) was around 20 μmol g^{-1}. It is interesting to observe that polycrystalline Pt/C catalyst showed a higher initial heat than preferentially oriented samples. It is well known that the heat of adsorption increases with decreasing average coordination number of the surface metal atoms, due to preferential adsorption on low coordination sites like edges and corners [38]. Thus, this finding would indicate that the amount of highly unsaturated platinum atoms and open faces in this catalyst is higher than in the preferentially oriented samples, which is compatible with the voltammetric and irreversible Bi and Ge adsorptions results described in the previous section.

The heat-coverage profiles were different for preferentially oriented Pt(100)/C and Pt(111)/C catalysts. The differential heats strongly decreased with coverage and, in both cases, the saturation coverage was reached at about 5 μmol g^{-1}. This result is coherent with the higher platinum particle size obtained for these samples (≈10 nm) as compared to Pt/C (≈3 nm), described in the TEM section. Although the CO adsorption capacity was similar for both samples, important differences were found in initial adsorption heats. Thus, Pt(111)/C showed a unusual high initial heat (107 kJ mol^{-1}), close to the typical values for polycrystalline Pt/C catalysts [36,39]. This result can be tentatively explained on the basis of a higher number of highly unsaturated platinum atoms present in this sample. In fact, the results of irreversible adsorption of Bi and Ge revealed the presence of a higher amount of low coordination surface atoms in Pt(111)/C as compared to Pt(100)/C, although this fact does not seem to be important enough to explain by itself the difference in initial heats (107 vs 90 kJ mol^{-1}). Furthermore, Pt(111)/C showed higher adsorption heats than Pt(100)/C in all range of CO coverages studied, not only in the initial region. The explanation for this behavior can be found taking into account the TEM and voltammetric results. Thus, Pt(100) particles showed a well defined cubic shape (Fig. 1B) with wide domains of (100) terraces, whereas Pt(111) nanoparticles presented a more faceted shape (Fig. 1C) with small (111) ordered surface domains and a noticeable amount of stepped surfaces and monoatomic steps connecting the (111) facets (prominent peak at 0.12 V in Fig. 2c). Thus, the presence of a larger amount of these linking sites with lower coordination number in Pt(111)/C could account for the higher adsorption heats showed by this sample.

3.4. Catalytic behavior

3.4.1. Crotonaldehyde hydrogenation

The performance of the catalysts (previously reduced at 473 K) was tested in the vapor phase hydrogenation of crotonaldehyde at 333 K. The evolution of catalytic activity (TOF, calculated in basis of CO uptakes at 300 K) with time on stream for the three catalysts studied is showed in Fig. 4. It can be seen that, after a period of 20 min with a strong deactivation, the activity remained quite stable with time. This fast deactivation of the catalysts is typical of this reaction [40] and has been previously related to the decarbonylation of the reactant molecule yielding carbon monoxide, which is irreversively adsorbed on platinum at the reaction conditions [20]. It can be clearly appreciated that the specific activity strongly depends on the platinum face exposed, which is a clear indicative of the structure-sensitive character of this reaction [41]. Fur-

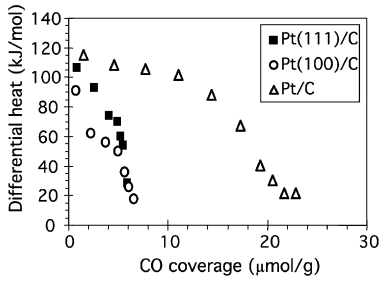

Fig. 3. Differential heats of CO adsorption at 300 K vs CO coverage for Pt/C, Pt(111)/C, and Pt(100)/C catalysts, previously reduced at 473 K.

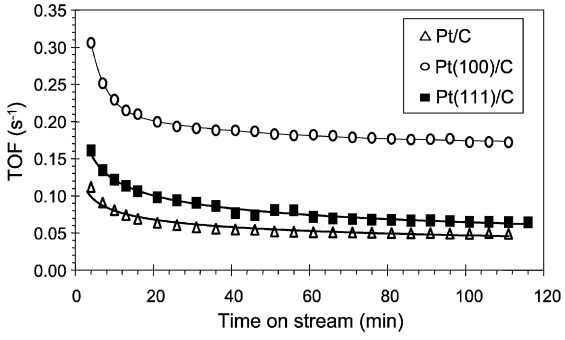

Fig. 4. TOF in crotonaldehyde hydrogenation at 333 K as a function of time on stream for Pt/C, Pt(111)/C, and Pt(100)/C catalysts.

thermore, it is interesting to observe that polycrystalline Pt/C showed lower TOF values than preferentially oriented catalysts. Englisch et al. [20], in a very complete work on structure sensitivity of crotonaldehyde hydrogenation over Pt/SiO_2, also found lower activity for catalysts with smaller metal particles, and this behavior was attributed to a faster deactivation caused by strong adsorption of crotonaldehyde on low coordination sites like edges and corners. However, this fact has not been detected in our case, and deactivation profiles were very similar for the three catalysts under study. In the same way, Singh et al. [42] found a 25-fold increase in TOF for citral hydrogenation as the average platinum crystallite size increases from 1 to 5 nm. Again, the higher participation of low coordination number surface atoms as the metal particle size decreases was invoked to explain this behavior. Note that these highly exposed atoms are assumed to be the most abundant on the surface of Pt/C as indicated by voltammetric and microcalorimetric results (see Figs. 2a and 3).

With regards to selectivity, the main product formed in all cases was the saturated aldehyde (butanal). Thus, the selectivity to the unsaturated alcohol was almost negligible for polycrystalline Pt/C and Pt(100)/C catalysts while Pt(111)/C showed certain selectivity to crotyl alcohol (4% molar fraction). It is well known that there is an effect of the metal morfology on the adsorption geometry of unsaturated aldehydes, leading to different types of reaction pathways and finally, different selectivities [43]. The theoretical calculations of Delbecq et al. [44] suggest that, in the case of (100) and open faces or steps, crotonaldehyde adsorption involves both double bonds, in a so-called η_4 planar coordination, this geometry leading to the preferential hydrogenation of the C=C bond for kinetic reasons. This fact would explain the low selectivity toward unsaturated alcohol found for Pt(100)/C and Pt/C catalysts, where the fraction of (100) facets and low coordinated atoms, respectively, is very high. On the other hand, the dense (111) metal faces are not favorable for the C=C coordination, and crotonaldehyde adsorption via carbonyl bond (di-$\sigma^{C=O}$) is energetically favored. Thus, a greater participation of these faces in the catalysts surface would improve the selectivity to unsaturated alcohol. The low value of selectivity obtained for Pt(111)/C in our study could be due to the presence of a noticeable fraction of stepped surfaces vicinal to (111) small domains (see prominent peaks at 0.12 and 0.26 V in Fig. 2c) since, in these surfaces, the crotonaldehyde coordination is shifted to a $\pi^{C=C}$ mode [43]. Furthermore, voltammetric results showed that the surface of Pt(111)/C is not exclusively participated by (111) facets and the presence of large (100) domains (peak at 0.37 V in Fig. 2c) could also be responsible of the low value of selectivity to unsaturated alcohol.

3.4.2. Cinnamaldehyde hydrogenation

Fig. 5 shows the main reaction pathways that can occur during cinnamaldehyde hydrogenation. Under the experimental conditions used in the present work only these four products were detected. Activity and selectivity of the catalysts in the hydrogenation of cinnamaldehyde were evaluated in the liquid phase at 383 K and 5 MPa. Fig. 6 plots the conversion of

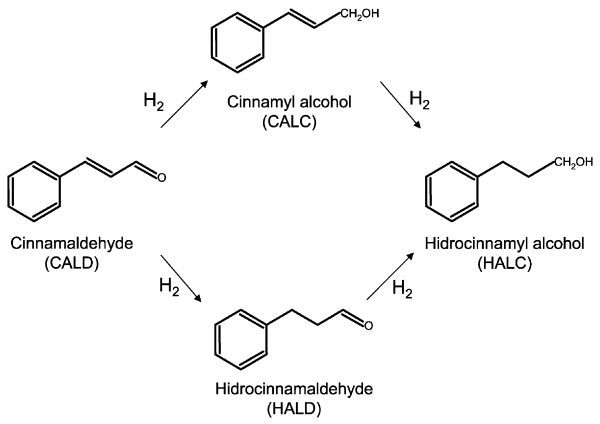

Fig. 5. Reaction scheme for cinnamaldehyde hydrogenation.

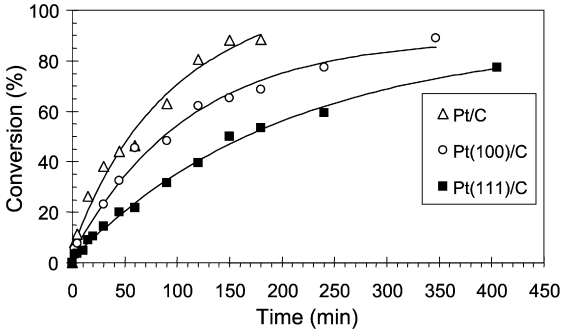

Fig. 6. Conversion of cinnamaldehyde as a function of time for Pt/C, Pt(111)/C, and Pt(100)/C catalysts.

Table 1
Rate constant, TOF and selectivity to the saturated aldehyde and the unsaturated alcohol at 10% conversion in cinnamaldehyde hydrogenation for Pt/C, Pt(111)/C, and Pt(100)/C catalysts

Catalyst	Rate constant (min^{-1})	TOF (s^{-1})	Selectivity (%)[a]	
			HALD	CALC
Pt/C	0.016	0.003	82	16
Pt(100)/C	0.008	0.040	61	36
Pt(111)/C	0.005	0.020	49	48

[a] Values at 10% conversion.

cinnamaldehyde as a function of reaction time for the three catalysts under study. Initial activities were expressed in term of rate constant (min^{-1}), which were obtained from the slope of the cinnamaldehyde concentration-time plot and considering a first rate law equation. The activity per active site (TOF) was calculated using the CO uptakes to determinate the number of surface metal sites and the results are summarized in Table 1. As it can be seen, both the rate constant (Table 1) and the conversion of cinnamaldehyde reached for similar reaction times (Fig. 6), followed the trend: Pt/C > Pt(100)/C > Pt(111)/C. However, when the rate is normalized by the number of accessible platinum atoms (TOF), the trend changes to: Pt(100)/C > Pt(111)/C > Pt/C which is consistent with that obtained in crotonaldehyde hydrogenation (Fig. 4).

Regarding the products distribution, again the main reaction product was the saturated aldehyde (HALD) although, conversely to crotonaldehyde hydrogenation, the three catalysts

under study yielded noticeable amounts of cinnamyl alcohol (CALC). This fact is not strange since it is well known that the selective hydrogenation of the carbonyl bond is more difficult to achieve when lower aldehydes are involved and the reaction takes place in gas phase [45]. Table 1 also shows the selectivity to cinnamyl alcohol (CALC) and hydrocinnamaldehyde (HALD) at equal conversion level (10%) for the three catalysts under study. It is interesting to observe that polycrystalline Pt/C showed lower selectivity to CALC than preferentially oriented samples. This fact can be explained in terms of particle size. It is well known that metal particle size has a strong influence in the selectivity to cinnamyl alcohol in the case of monometallic platinum catalysts [46]. Thus, the selectivity for C=O hydrogenation increased with increasing crystallite size. Note that Pt/C showed an average platinum particle size of 3 nm while in preferred oriented samples, Pt(100)/C and Pt(111)/C, platinum is in form of large particles of around 10 nm size (see Fig. 1). Repulsive interactions between the phenyl ring and the large metal crystallites, which hinders the interaction via the C=C bond and enhances interaction via C=O bond, is proposed to explain this behavior. This effect is absent in the case of small metal particles because both double bonds, C=C and C=O, could approach the surface with less repulsive interactions between the phenyl ring and the metal surface [47].

Furthermore, it can be seen in Table 1 that Pt(111)/C showed higher selectivity to CALC than Pt(100)/C (48 vs 36%). In this case no size effect can be invoked since both samples showed similar average particle size (10 nm). However, as pointed before, both catalysts differ in the facets distribution of the metal particles, with a higher ratio of (111) domains in the case of Pt(111)/C. Thus, these results clearly indicate that, besides a size effect, the amount of (111) facets composing the metal particle play a crucial role in increasing the selectivity to unsaturated alcohol in these kind of reactions. In this way, previous studies on prenal hydrogenation on well-defined (111) [48] and (110) [49] platinum surfaces, found that the main product (also at 10% conversion) was the unsaturated alcohol and the saturated aldehyde, respectively. Interestingly, the same authors also found that prenal hydrogenation on Pt(553) (which can be considered as a surface with (111) terraces and steps) resulted in a lower selectivity to the unsaturated alcohol compared to (111) flat surface [50]. Again, the simultaneous presence of (111) terraces (where the di-$\sigma^{C=O}$ adsorption mode is preferred) and steps ($\pi^{C=C}$ adsorption mode preferred) is invoked to explain the lower selectivity to the unsaturated alcohol on this stepped surface. As already seen, it has been proved that the platinum particles composing Pt(111)/C have a noticeable amount of stepped surfaces vicinal to (111) small domains (Fig. 2c), which would explain the noticeable yield of saturated aldehyde (49% HALD, Table 1) obtained for this sample. It is necessary to bear in mind that substituents at the C=C bond have a strong influence on the selectivity to the unsaturated alcohol and thus, can influence the intrinsic selectivity determined by the platinum surface. Thus, is not strange that some works, based on the hydrogenation of the simplest unsaturated aldehyde (acrolein), introduced some new points to the factors controlling the selectivity in this kind of reactions. In a recent theoretical work, Loffreda et al. [51] concluded that the key point which determines the selectivity to allyl alcohol on Pt(111) is not the adsorption mode of the aldehyde, but the competitive desorption process of the half hydrogenated products (unsaturated alcohol vs saturated aldehyde). Furthermore, in contradiction with earlier assumptions, Mohr et al. [52] claim that the surface sites responsible of the C=O hydrogenation are the highly unsaturated surface atoms situated at corners and edges, although these conclusions are obtained for a very special catalytic system (Au/ZnO), and the same authors indicated that these conclusions could not be transferred to other catalytic systems.

4. Conclusions

The effect of the surface structure/shape of Pt nanoparticles on the crotonaldehyde and cinnamaldehyde hydrogenation reactions has been evaluated. Polyoriented and preferentially oriented (100) and (111) Pt nanoparticles have been synthesized and characterized by electrochemical and microcalorimetric techniques. TEM images of the corresponding Pt nanoparticles show semi-spherical, cubic and tetrahedral/hexagonal preferential shapes, respectively. Cyclic voltammetry results confirm the existence of a preferentially (100) and (111) surface orientation. In the case of the smallest Pt nanoparticles (3 nm), the presence of a polyoriented surface orientation is also confirmed by cyclic voltammetry. Furthermore, irreversible adsorption Bi and Ge, as well as CO adsorption microcalorimetry, suggested that the surface of polyoriented Pt/C is essentially constituted of highly unsaturated platinum atoms, situated at corners and edges. Catalytic activity in crotonaldehyde and cinnamaldehyde hydrogenations, expressed as TOF, showed a strong dependence with the face exposed, which is indicative of the structure sensitive character of these reactions. Moreover, Pt(111)/C showed higher selectivities to unsaturated alcohol than Pt/C and Pt(100)/C. A greater ratio of (111) facets in the surface of this catalyst is proposed to explain the observed results.

Acknowledgments

Financial support from the Ministerio de Educación y Ciencia (Spain) (Projects MAT2004-03480-C02-02, CTQ2006-04071 and NAN2004-09267-C05-05), the Network of Excelence InsidePores (European Commission Contract No. NMP3-CT2004-500895) and Generalitat Valenciana (acomp07/052) is gratefully acknowledged.

References

[1] A. Wieckowski, E. Savinova, C. Vayenas (Eds.), Catalysis and Electrocatalysis at Nanoparticle Surfaces, Dekker, New York, 2003.
[2] A. Wieckowski (Ed.), Interfacial Electrochemistry, Theory, Experiments and Applications, Dekker, New York, 1998.
[3] E. Herrero, J.M. Feliu, A. Aldaz, in: A.J. Bard, M. Stratmann (Eds.), Encyclopedia of Electrochemistry, vol. 2, Wiley–VCH, Weinheim, 2003, p. 443.
[4] M. Boudart, Adv. Catal. 20 (1969) 153.
[5] G.A. Somorjai, Adv. Catal. 26 (1977) 1.
[6] R. Narayanan, M.A. El-Sayed, Langmuir 21 (2005) 2027.

[7] R. Narayanan, M.A. El-Sayed, J. Am. Chem. Soc. 126 (2004) 7194.
[8] R. Narayanan, M.A. El-Sayed, Nano Lett. 4 (2004) 1343.
[9] R. Narayanan, M.A. El-Sayed, J. Phys. Chem. B 108 (2004) 5726.
[10] W.J. Yoo, S.M. Lee, H.T. Kim, M.A. El-Sayed, Bull. Korean Chem. Soc. 25 (2004) 843.
[11] W.J. Yoo, D. Hathcock, M.A. El-Sayed, J. Catal. 214 (2003) 1.
[12] R.M. Rioux, H. Song, M. Grass, S. Habas, K. Niesz, J.D. Hoefelmeyer, P.Yang, G.A. Somorjai, Top. Catal. 39 (2006) 167.
[13] H. Lee, S.E. Habas, S. Kweskin, D. Butcher, G.A. Somorjai, P. Yang, Angew. Chem. Int. Ed. 45 (2006) 7824.
[14] F.J. Vidal-Iglesias, J. Solla-Gullón, P. Rodríguez, E. Herrero, V. Montiel, J.M. Feliu, A. Aldaz, Electrochem. Commun. 6 (2004) 1080.
[15] J. Solla-Gullón, F.J. Vidal-Iglesias, E. Herrero, J.M. Feliu, A. Aldaz, Electrochem. Commun. 8 (2006) 189.
[16] T.S. Ahmadi, Z.L. Wang, T.C. Green, A. Henglein, M.A. El-Sayed, Science 272 (1996) 1924.
[17] T.S. Ahmadi, Z.L. Wang, A. Henglein, M.A. El-Sayed, Chem. Mater. 8 (1996) 1161.
[18] J.M. Petroski, Z.L. Wang, T.C. Green, M.A. El-Sayed, J. Phys. Chem. 102 (1998) 3316.
[19] T.K. Sau, C.J. Murphy, J. Am. Chem. Soc. 126 (2004) 8648.
[20] M. Englisch, A. Jentys, J.A. Lercher, J. Catal. 166 (1997) 25.
[21] G.F. Santori, M.L. Casella, G.J. Siri, H.R. Adúriz, O.A. Ferreti, React. Kinet. Catal. Lett. 75 (2002) 225.
[22] M.A. Vannice, B. Ben, J. Catal. 115 (1989) 65.
[23] N.R. Jana, L. Gearheart, C.J. Murphy, J. Phys. Chem. B 105 (2001) 4065.
[24] J. Solla-Gullón, V. Montiel, A. Aldaz, J. Clavilier, J. Electronal. Chem. 491 (2000) 69.
[25] J. Solla-Gullón, A. Rodes, V. Montiel, A. Aldaz, J. Clavilier, J. Electroanal. Chem. 554 (2003) 273.
[26] J. Solla-Gullón, V. Montiel, A. Aldaz, J. Clavilier, J. Electrochem. Soc. 150 (2003) E104.
[27] J.C. Serrano-Ruiz, G.W. Huber, M.A. Sánchez-Castillo, J.A. Dumesic, F. Rodríguez-Reinoso, A. Sepúlveda-Escribano, J. Catal. 241 (2006) 378.
[28] B.E. Spiewak, J.A. Dumesic, Thermochim. Acta 290 (1996) 43.
[29] Z.L. Wang, J. Phys. Chem. 104 (2000) 1153.
[30] J. Clavilier, R. Faure, G. Guinet, R. Durand, J. Electroanal. Chem. 107 (1980) 205.
[31] G.A. Attard, J.E. Gillies, C.A. Harris, D.J. Jenkins, P. Johnston, M.A. Price, D.J. Watson, P.B. Wells, Appl. Catal. A Gen. 222 (2001) 392.
[32] J. Solla-Gullón, F.J. Vidal-Iglesias, P. Rodríguez, E. Herrero, J.M. Feliu, J. Clavilier, A. Aldaz, J. Phys. Chem. B 108 (2004) 13573.
[33] P. Rodríguez, E. Herrero, J. Solla-Gullón, F. Vidal-Iglesias, A. Aldaz, J.M. Feliu, Electrochim. Acta 50 (2005) 3111.
[34] P. Rodríguez, E. Herrero, J. Solla-Gullón, F. Vidal-Iglesias, A. Aldaz, J.M. Feliu, Electrochim. Acta 50 (2005) 4308.
[35] P. Rodríguez, J. Solla-Gullón, F.J. Vidal-Iglesias, E. Herrero, A. Aldaz, J.M. Feliu, Anal. Chem. 77 (2005) 5317.
[36] J. Silvestre-Albero, J.C. Serrano-Ruiz, A. Sepúlveda-Escribano, F. Rodríguez-Reinoso, Appl. Catal. A Gen. 292 (2005) 244.
[37] A. Guerrero-Ruiz, A. Maroto-Valiente, M. Cerro-Alarcón, B. Bachiller-Baeza, I. Rodríguez-Ramos, Top. Catal. 19 (2002) 303.
[38] J.L. Gland, M.R. Maclellan, F.R. McFeely, J. Vac. Sci. Techol. A 1 (1983) 1070.
[39] J.C. Serrano-Ruiz, A. Sepúlveda-Escribano, F. Rodríguez-Reinoso, J. Catal. 246 (2007) 158.
[40] A. Waghray, D.G. Blackmond, J. Phys. Chem. 97 (1993) 6002.
[41] P. Gallezot, D. Richard, Catal. Rev. Sci. Eng. 40 (1998) 81.
[42] U.K. Sing, M.A. Vannice, Appl. Catal. A Gen. 213 (2001) 1.
[43] P. Sautet, Top. Catal. 13 (2000) 213.
[44] F. Delbeq, P. Sautet, J. Catal. 152 (1995) 217.
[45] P. Claus, Top. Catal. 5 (1998) 51.
[46] A. Giroir-Fendler, P. Gallezot, D. Richard, Catal. Lett. 5 (1990) 169.
[47] S. Galvagno, G. Capannelli, J. Mol. Catal. 64 (1991) 237.
[48] T. Birchem, C.M. Pradier, Y. Berthier, G. Cordier, J. Catal. 146 (1994) 503.
[49] C.M. Pradier, T. Birchem, Y. Berthier, G. Cordier, Catal. Lett. 29 (1994) 371.
[50] T. Birchem, C.M. Pradier, Y. Berthier, G. Cordier, J. Catal. 161 (1996) 68.
[51] D. Loffreda, F. Delbecq, F. Vigné, P. Sautet, J. Am. Chem. Soc. 158 (2006) 1316.
[52] C. Mohr, H. Hofmeister, P. Claus, J. Catal. 213 (2003) 86.